

Extracting Diagnosis Pathways from Electronic Health Records using Deep Reinforcement Learning

Lillian Muyama

Inria Paris, Paris, France

*Centre de Recherche des Cordeliers, Inserm, Université Paris Cité,
Sorbonne Université, Paris, France*

LILLIAN.MUYAMA@INRIA.FR

Antoine Neuraz*

Hôpital Necker, Assistance Publique - Hôpitaux de Paris, Paris, France

*Centre de Recherche des Cordeliers, Inserm, Université Paris Cité,
Sorbonne Université, Paris, France*

ANTOINE.NEURAZ@APHP.FR

Adrien Coulet*

Inria Paris, Paris, France

*Centre de Recherche des Cordeliers, Inserm, Université Paris Cité,
Sorbonne Université, Paris, France*

ADRIEN.COULET@INRIA.FR

Abstract

Clinical diagnosis guidelines aim at specifying the steps that may lead to a diagnosis. Inspired by guidelines, we aim to learn the optimal sequence of actions to perform in order to obtain a correct diagnosis from electronic health records. We apply various deep reinforcement learning algorithms to this task and experiment on a synthetic but realistic dataset to differentially diagnose anemia and its subtypes and particularly evaluate the robustness of various approaches to noise and missing data. Experimental results show that the deep reinforcement learning algorithms show competitive performance compared to the state-of-the-art methods with the added advantage that they enable the progressive generation of a pathway to the suggested diagnosis, which can both guide and explain the decision process.

Keywords: Clinical Diagnosis Pathway, Reinforcement Learning, Deep Q-Network, Anemia

1. Introduction

Clinical diagnosis guidelines are documents to guide, rationalize and normalize clinical decisions, classically established by a college of experts on the basis of the best available evidence (Field et al., 1990). They mainly describe the steps that may lead to a diagnosis, such as information collection, observations, and

laboratory test orders. However, clinical guidelines suffer several drawbacks. First, they are designed to cover the majority of the population and hence may fail to guide to the right diagnosis in the case of uncommon patients such as those with multiple diseases. Second, their establishment is long and expensive, and updating them is usually done after several years (Steinberg et al., 2011). This makes them unsuitable to fast emerging practices such as those associated with a recently developed laboratory test or an emerging disease. Moreover, as clinical guidelines are expensive and time-consuming to produce, this development approach does not scale to the full spectrum of diseases. Thus, more versatile and scalable methods are required to provide insights when clinical guidelines are not available.

We think that machine learning approaches trained on clinical data may complement diagnosis guidelines. In particular, we aim at developing approaches able to guide each step of the decision process, as described in Adler-Milstein et al. (2021). We believe that such an approach may reduce the number of irrelevant tests therefore optimizing healthcare costs, but primarily may propose more personalized and accurate diagnoses, especially in the case of patients with uncommon conditions.

The collection of patient-level data in Electronic Health Records (EHRs) offers great opportunities to gain knowledge about clinical practice (Jensen et al., 2012). EHRs encompass structured, semi-structured

* These authors contributed equally

and unstructured data about patients' health such as medications, laboratory test orders and results, diagnoses, as well as demographic features. Previous works have trained machine learning (ML) methods on EHRs to automatically suggest diagnoses for patients such as in [Lipton et al. \(2015\)](#), [Miotto et al. \(2016\)](#) and [Choi et al. \(2016\)](#). However, in these studies, supervised ML methods are employed to predict a unique endpoint, *i.e.*, the diagnosis represented as a class label. We believe that for data-driven approaches to find adoption in clinical practice, it is important for a diagnosis not to be limited to an endpoint, but to be represented as a pathway that follows steps of medical reasoning and decision-making.

In this work, we propose to leverage EHR data and investigate how it can be used to train a family of Reinforcement Learning (RL) methods to build explainable pathways for the differential diagnosis of anemia, as a primary use case. Anemia is a clinical condition defined as a lower-than-normal amount of healthy red blood cells in the body, which we chose for three reasons: its diagnosis is made mainly from a series of laboratory tests that are available in most EHRs; it is a common diagnosis implying that the associated amount of data may be sufficient to train RL models; and the differential diagnosis of anemia is frequently complex to establish, making its guidance useful.

We propose to use RL because it builds a model that is able to pass through various *actions* and *states* to reach a final objective state. We adapted the framework of RL to construct individualized pathways of observations in a step-by-step manner, in order to suggest a decision. In our particular use case, a pathway is a sequence of laboratory test requests (actions), whose results are then obtained (states) before either requesting for another test or terminating on an anemia differential diagnosis. We make the assumption that the constructed pathways can complement clinical guidelines to aid practitioners in decision-making during the diagnosis process.

Our main contributions are: *(i)* an adaptation of the RL framework to progressively construct optimal sequences of actions to perform in order to reach a diagnosis and *(ii)* an empirical analysis that identifies the most suitable algorithm for our use-case, and evaluates the robustness of our approach in regards to levels of missing and noisy data.

2. Related Work

Previously, studies have used various process mining, machine learning and statistical methods to extract clinical pathways from medical data. [Zhang et al. \(2015\)](#) proposed Markov Chains for the identification of clinical pathways using patient visits data. [Perer et al. \(2015\)](#) extracted common patterns in the data in order to build pathways while [Baker et al. \(2017\)](#) used a Markov model to extract meaningful clinical events from patient data. [Huang et al. \(2013, 2014, 2018\)](#) took a more statistical approach to build treatment pathways by using a Latent Dirichlet Allocation-based method. Machine learning methods such as Long Short-Term Memory and reinforcement learning have also been used to construct pathways for optimal treatment in several use-cases such as in [Lin et al. \(2021\)](#) and [Li et al. \(2022\)](#) respectively. However, the focus of all these papers is building pathways for the *treatment* of patients with a specific medical condition. In our paper, we aim to build pathways for the *diagnosis* of medical conditions.

Likewise, numerous studies have leveraged machine learning methods for disease diagnosis. Given the longitudinal nature of Electronic Health Record (EHR) data, a prevalent choice in these investigations has been Recurrent Neural Networks (RNNs), as observed in the works of [Lipton et al. \(2015\)](#) and [Choi et al. \(2016\)](#). Additionally, RNNs have also been used in the prediction of future patient outcomes such as in [Koshimizu et al. \(2020\)](#). In [Obaido et al. \(2022\)](#), [Zoabi et al. \(2021\)](#) and [Kavya et al. \(2021\)](#), they go further by not only employing ML approaches to provide clinical diagnoses for the patients, but also using explainable Artificial Intelligence (AI) methods to interpret the model results. However, our aim is not only to diagnose the patient with the correct condition, but also to find the optimal sequence of features to test to reach this diagnosis for each patient. In other terms, our aim is to construct personalized diagnosis pathways that delineate the steps leading to the diagnosis, thereby explaining the diagnostic process.

Previous works used reinforcement learning methods for costly feature acquisition in classification tasks such as in [Li and Oliva \(2021\)](#) and [Janisch et al. \(2019\)](#). However, these works did not primarily focus on the clinical diagnosis task. [Yu et al. \(2023\)](#) aimed to optimize the financial cost of the three prediction tasks, including the prediction of Acute Kidney Injury, using RL. While it was shown that their method

reduced the cost of diagnosis, the actions taken at each step in the diagnosis process were not shown, therefore the pathways' overall relevance and explainability were unknown. In addition, Tang et al. (2016), Wei et al. (2018) and Kao et al. (2018) used RL to diagnose patients by inquiring about the presence of disease-related symptoms from users. While our approach similarly formulates the diagnosis process as a sequential decision-making problem and applies deep reinforcement learning (DRL) techniques, these studies use a symptom self-checking approach, whereas we aim to use EHR data. We believe that our approach is more suitable as EHRs encompass data collected routinely in clinical practice, including objective and normalized measurements such as laboratory results which we are proposing to use in this first study.

3. Methods

3.1. Decision Problem

We consider the anemia diagnosis process as a sequential decision-making problem and formulate it as a Markov Decision Process (MDP) (Littman, 2001), following the RL (Sutton and Barto, 2018) paradigm. Accordingly, we define an *agent* interacting with an *environment* in order to maximize a cumulative reward signal. At each time step t , the agent receives an observation o from the environment *state*, takes an *action*, and obtains a *reward*. The goal is to learn a policy, *i.e.*, a function that maps states to actions, that maximizes the reward signal. In this study, our agents are taking observations from the synthetic EHRs of a Clinical Data Warehouse (CDW), in order to reach a diagnosis, which is a final action. Let \mathcal{D} denotes a dataset of size $n \times (m + 1)$, associated with F , the set of names of the m features, and C the set of possible diagnosis values. An instance D^i in \mathcal{D} is a pair (X^i, Y^i) with $X^i = \{x_1^i, \dots, x_j^i, \dots, x_m^i\}$ where x_j^i is the value of the feature j for the patient i , m is the total number of features and $Y^i \in C$ is the anemia diagnosis of patient i . Accordingly, our MDP is defined by the quadruple (S, A, T, R) as follows:

- S is the set of states. At each timestep, the agent receives an observation o of the state s_t , which is a vector of fixed size m comprising the values of the features that have already been queried by the agent at time t ; features that have not been queried yet are associated with the value -1. Equation 1 defines the j^{th} element of o , where

F' denotes the set of features that have already been queried by the agent.

$$o_j = \begin{cases} x_j, & \text{if } f_j \in F' \\ -1, & \text{otherwise.} \end{cases} \quad (1)$$

- A is the set of possible actions, which is the union of the set of *feature value acquisition actions*, A_f (or value actions for short), and the set of *diagnostic actions*, A_d . At each time step, the agent takes one action $a_t \in A$. Actions from A_f are taking values from the set of features F . Accordingly a specific value $f_j \in F$ will trigger the action of querying for the value of this feature from the CDW. Actions from A_d are taking values from the set of possible diagnoses C . At a time step, if $a_t \in A_d$, the episode is terminated. Also, if an episode reaches the number of maximum specified steps without reaching a diagnosis, it is terminated.
- T denotes the transition function that gives the probability of moving from a state s_t to a state s_{t+1} given an agent action $a_t \in A$.
- R is the reward function. r_{t+1} , which can be written as $R(s_t, a_t)$, is the immediate reward when an agent takes an action a_t in a state s_t . In the case of a diagnostic action $a_t \in A_d$, if the diagnosis is correct, the reward is +1, otherwise the reward is -1. For a value action $a_t \in A_f$, if the feature has already been queried, the agent receives a reward of -1 and the episode is terminated. Otherwise, the agent receives a reward of 0. Accordingly, the reward functions for diagnostic and value actions, are formalized as follows:

$$\text{if } a_t \in A_d, R(s_t, a_t) = \begin{cases} 1, & \text{if } a_t = Y^i \\ -1, & \text{otherwise} \end{cases} \quad (2)$$

$$\text{if } a_t \in A_f, R(s_t, a_t) = \begin{cases} -1, & \text{if } a_t \in F' \\ 0, & \text{otherwise.} \end{cases} \quad (3)$$

3.2. Q-learning and Extensions

Q-learning (Watkins and Dayan, 1992) is an RL algorithm that outputs the best action to take in a given state based on the expected future reward of taking that action in that particular state. The expected future reward is named the Q-value of that

state-action pair, noted $Q(s, a)$. At each time step, the agent selects an action following a policy π , and the goal is to find the optimal policy π^* that maximizes the reward function. During model training, the Q-values are updated using the Bellman Equation as described in Appendix A, equation 4.

In our use case, since the state space is large and continuous, we propose to use a **Deep Q-Network (DQN)** Mnih et al. (2015) which uses a neural network to approximate the Q-value function. In order to improve DQN stability and performance, several extensions of the DQN algorithm have been developed. Particularly **Double DQN (DDQN)**, **Dueling DQN** and **Prioritized Experience Replay (PER)**, which we use in the following of this paper and briefly describe in Appendix A. These techniques enhance the performance of the DQN algorithm by improving its stability, making the learning process faster and more efficient, and reducing overestimation bias, among other benefits.

3.3. State-of-the-Art Classifiers

As part of the study, we compared the performance of the DRL models with four classical supervised learning algorithms that are commonly used for classification tasks, namely Decision Tree (DT), Random Forest (RF), Support Vector Machine (SVM), and a Feed-Forward Neural Network (FFNN). DT has a particular status in our study for two reasons. First, we experimented on synthetic data, whose labels were assigned according to a decision tree. For this reason, the DT approach is expected to perform very well on our data. Second, DT is the only considered classifier that is self-explanatory as the path in the decision tree that is taken to classify an instance constitutes a pathway to the diagnosis.

3.4. Dataset Synthesis

In order to develop and evaluate the performance of our various agents, we built a synthetic dataset. Firstly, we identified a set of relevant variables from existing literature about the diagnosis of different anemia sub-types and after discussions with a domain expert. This concluded with the identification of 17 features and 8 anemia classes. Secondly, we constructed a dataset for each anemia class based on the decision tree adapted from the literature and presented in Figure B.1. The values for each feature were generated using a uniform probability distribution. The final dataset comprises feature values for 70,000

patients. A more detailed description of the dataset synthesis is in Appendix B. The class distribution is illustrated in Figure B.2; the ratio of observed *vs.* missing values for each feature is shown in Figure B.3; descriptive statistics of the dataset are shown in Table B.1; and an example of an instance from the dataset is provided Table B.2.

Additionally, in order to compare the robustness of various approaches to imperfect data, we defined functions to artificially introduce different levels of noisiness and missingness to our training dataset as described in section B.3 of the Appendices.

3.5. Evaluation Approach and Implementation

80% of the dataset was used to train the model while 20% was used as the test set. Additionally, 10% of the training dataset (8% of the dataset) was used for validation. The validation and test sets used in all the experiments are constant *i.e.*, without noise or missingness. Only training sets are changed.

The primary metric used for evaluating the performance of our models is the *accuracy*, which is the ratio of episodes that terminated with a correct diagnosis. We further computed the average number of actions performed for each episode, displayed as the *mean episode length*. This is not applicable to the state-of-the-art classifiers since those consider all available features. The *F1* and *ROC-AUC* scores were also computed using a one-vs-rest approach and macro-averaging. Ten runs were conducted for the first experiment comparing DQN approaches and five runs for the subsequent experiments on the models' robustness. Each run was performed with the same datasets but with different seeds, which influence the models' interactions with the environment as well as their initial weights.

We used the OpenAI Gym Python library (Brockman et al., 2016) to implement our environment. To build our agents, we used the stable-baselines package (Hill et al., 2018), and the values of the hyperparameters are as shown in Table C.1 in Appendix C. They were chosen through prior knowledge, existing literature, and experimentation. The hyperparameters for the SOTA models were chosen using a grid search strategy. The source code is available at https://github.com/lilly-muyama/anemia_diagnosis_pathways.

4. Results

4.1. Performance Comparison of DQN and its extensions

In the first round of experiments, we trained DQN, Double DQN, Dueling DQN and Dueling Double DQN on our dataset; and also enabled prioritized experience replay (PER) for each of these models. We also trained a Proximal Policy Optimization (PPO) algorithm using a similar number of timesteps for comparison purposes. The associated results are compiled in Table 1. Model names associated with the suffix -PER correspond to the mentioned DQN extension together with PER. In order to gauge the stability, for each model, we conducted ten different runs of the same experiment using different seeds. The values in Table 1 are therefore averages and standard deviations (SD) over the ten runs. The number of time steps used was determined in the first run using the validation data and remained constant for the other nine runs.

Dueling DQN-PER provided the best accuracy and the second lowest SD, while Dueling DDQN-PER exhibited a similar performance with slightly lower accuracy and slightly less variance. For these reasons, we used only these two DQN models for the rest of the experiments.

4.2. Performance Comparison with SOTA classifiers

The results of these experiments are shown in Table 2. Since diagnosis labels of the synthetic dataset are assigned following the decision tree in Figure B.1, the tree-based agent, which is based on the same tree achieved a perfect score. Also, we built an agent that acts randomly at each timestep for comparison purposes. Because the SOTA classifiers use a constant set of features to make a diagnosis, they do not have a mean episode length. The tree-based algorithms and the FFNN performed better than the DQN models, while SVM had a lower performance.

4.3. Varying levels of missing data and noisiness

Figure 1(a) depicts the accuracy when the level of missingness added to the training dataset varies. All the models' performance declined at a steady rate, with the DQN models' accuracy declining more slowly than the rest. SVM had the speediest deterioration. Figure 1(b) shows the accuracy when the

level of noise in the training set varies. SVM showed the sharpest decline, while the rest of the models performed comparably, and the Dueling DQN-PER model exhibited a consistent performance across all noise levels. Figure 1(c) is similar to Figure 1(a) as it depicts the varying accuracy as the level of missingness increases but with a fixed level of noise of 0.2. Once more, SVM performance declined rapidly and the DT's performance decreased faster than the DQN models or the other classifiers. The two DQN models exhibited a consistent performance. The depicted accuracy in Figures 1(a)-1(c) is the median of the accuracy as five runs were conducted for these experiments.

4.4. Varying the size of train sets

In order to understand whether this method can be applied to the diagnosis of conditions where data may be scarce, such as with rare diseases, we conducted experiments with train sets of different sizes. For each size, a fraction of the train set was randomly selected and removed, leaving the remaining data to form the new set. Runs were repeated five times for each size of the train set, whereby a different subset was removed each time. The Dueling DDQN-PER model was used for these experiments and for each run, the same number of timesteps was used. Figure 1(d) shows the mean accuracy for each train set size. The shaded region represents the 95% confidence interval. The RF classifier is also depicted in the figure for comparison and it was chosen for its stability and high performance. As depicted, the DQN model was able to learn the clinical pathways and diagnose the patients. However, for all train set sizes, its performance was lower than the RF and as the size of the train set decreased, the model's performance became less stable.

5. Discussion

As illustrated by our study, applying deep reinforcement learning methods to EHR data can be used to learn clinical diagnosis pathways for patients whereby at each step, a different action is taken by the agent until a diagnosis is reached. In comparing our two best DQN models to state-of-the-art classifiers, while the latter perform extremely well on perfect data, the two DQN models performed comparably and sometimes better on imperfect data, showing their robustness. Furthermore, using different training sizes, the

Table 1: Performance of the RL models.

Model	Accuracy	Mean episode length	F1	ROC-AUC
PPO	25.575 ± 16.537	1.628 ± 0.852	18.422 ± 25.227	54.733 ± 16.172
DQN	89.309 ± 14.684	4.272 ± 0.449	88.728 ± 15.946	93.904 ± 8.280
DDQN	92.792 ± 5.370	4.660 ± 0.312	92.183 ± 6.249	95.742 ± 3.278
Dueling DQN	92.459 ± 5.313	4.697 ± 0.239	91.722 ± 6.568	95.645 ± 3.266
Dueling DDQN	77.147 ± 31.987	4.444 ± 1.018	74.358 ± 34.975	86.842 ± 18.059
DQN-PER	93.708 ± 5.509	4.673 ± 0.288	93.615 ± 5.195	96.412 ± 3.034
DDQN-PER	95.571 ± 2.007	4.917 ± 0.355	95.336 ± 2.115	97.459 ± 1.163
Dueling DQN-PER	96.639 ± 1.462	4.588 ± 0.201	96.498 ± 1.515	98.106 ± 0.823
Dueling DDQN-PER	96.330 ± 1.316	4.821 ± 0.448	96.168 ± 1.351	97.863 ± 0.813

Table 2: Performance of the DQN and the state-of-the-art classifiers. The tree-based agent has a perfect score because it acts according to the decision tree used to build the dataset

Model	Accuracy \pm SD	Mean episode length	F1	ROC-AUC
Random Agent	12.343 ± 0.331	1.534 ± 0.009	12.337 ± 0.326	49.996 ± 0.204
Tree-based Agent	100.000 ± 0.000	3.975 ± 0.000	100.000 ± 0.000	100.000 ± 0.000
Decision Tree	99.960 ± 0.004	N/A	99.961 ± 0.004	99.979 ± 0.002
Random Forest	99.897 ± 0.012	N/A	99.898 ± 0.011	99.946 ± 0.006
FFNN	97.966 ± 0.274	N/A	97.914 ± 0.281	98.806 ± 0.161
SVM	94.893 ± 0.000	N/A	94.363 ± 0.000	96.795 ± 0.000
Dueling DQN-PER	96.639 ± 1.462	4.588 ± 0.201	96.498 ± 1.515	98.106 ± 0.823
Dueling DDQN-PER	96.330 ± 1.316	4.821 ± 0.448	96.168 ± 1.351	97.863 ± 0.813

DQN Models showed their capacity to learn clinical diagnosis pathways associated with decent performance, even in the context of reasonably small-sized datasets.

5.1. Generated Pathways

Besides quantitative evaluation, the pathways constructed by DQN models present two qualities. The fact that they are composed of progressive observations that lead to a diagnostic decision, makes them explainable: One may understand why a particular diagnosis is reached by looking at the sequence of features selected and their associated values. In addition, the set of pathways generated by a test set can be aggregated to generate a data structure similar to diagnosis guidelines. We note that the DT algorithms are also intrinsically explainable, but our results show that they are less robust to imperfect data. Sample generated pathways are shown in Appendix D. Interactive plots of the pathways

generated by the model can be accessed at <https://lilly-muyama.github.io/>.

5.2. DQN Algorithms Performance

From Table 1, DDQN and Dueling DQN exhibit similar performance and illustrate that both extensions improve the accuracy and stability of the standard DQN. However, Dueling DDQN exhibited the lowest performance of all the algorithms and showed wide variability. This may be because both Double DQN and Dueling DQN were created to solve the same problem: the overestimation of Q-values. Therefore, using both techniques at the same time may not lead to better performance as long as the Q-value is still estimated using the same technique as in Double DQN. Additionally, using both Double DQN and Dueling DQN at the same time makes the model more complex, which may result in further instability.

It is also important to note that for each of the four algorithms discussed above, combining them with

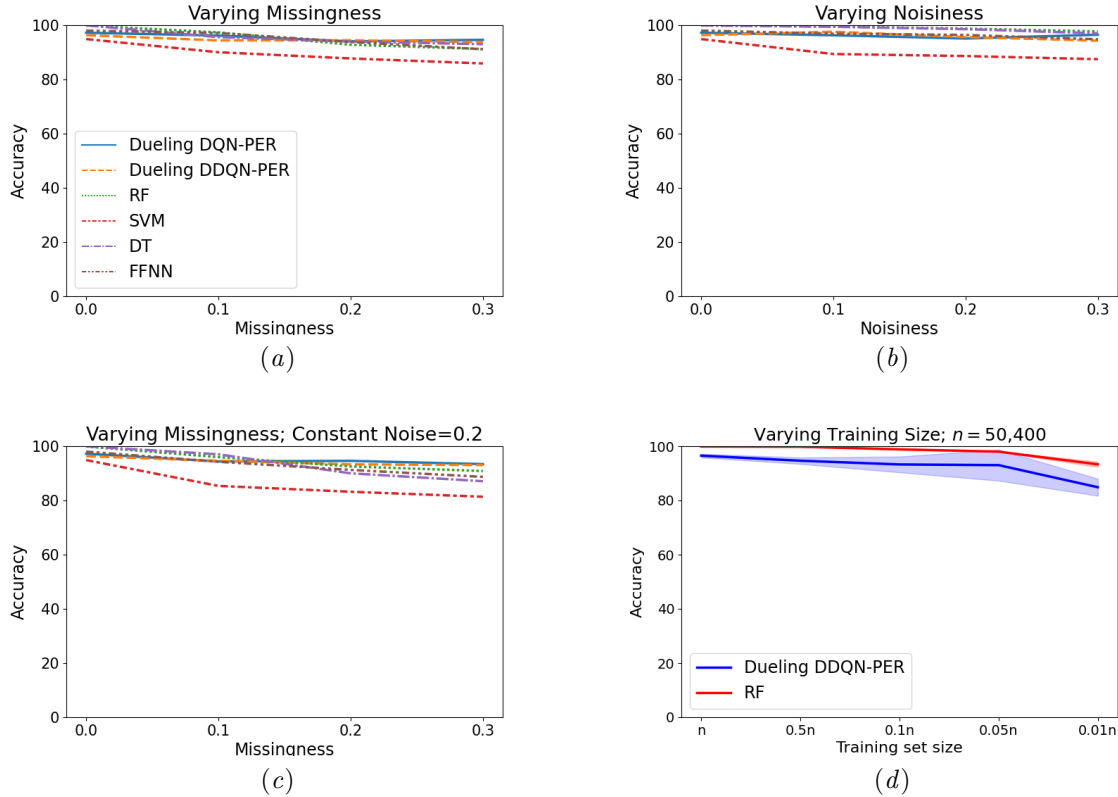


Figure 1: Accuracy of approaches with varying levels of missingness, noisiness, and train set size. The graphs show the accuracy (median) of the models at different (a) missingness levels; (b) noisiness levels; (c) missingness levels at a constant noisiness level (0.2). (d) shows the accuracy (mean) and the 95% confidence interval of the models based on the size of the train set.

Prioritized Experience Replay resulted in better results both in terms of mean and SD of the accuracy. This is explained by the fact that in DQN, Double DQN, and Dueling DQN, during training, the experiences are sampled uniformly from the replay buffer. However, PER prioritizes these experiences such that those with a higher priority are sampled more often. Effectively, in a task such as ours, where most of the actions have a zero reward, this type of DQN favors transitions with a non-zero reward that are mainly the diagnosis actions. Sampling these actions more frequently, on which the accuracy is primarily based, leads the model to learn more and faster about them.

5.3. Quality of Diagnoses

Regarding the comparison with SOTA classifiers, since we built our dataset using a decision tree, it

was expected that the tree-based classifiers would perform extremely well. The performance of the two DQN Models was slightly lower than those of the tree-based methods and the neural network, while SVM had slightly lower performance.

In Table 3, we display the classification report of one particular experiment with the Dueling DQN-PER model, with an accuracy of 97.186, which is the closest accuracy to the mean. The report shows that most of the anemia classes exhibited a decent performance. However, while the *No anemia* class had the best recall with a perfect score of 1, it also had the lowest precision at 0.92, meaning that several instances were being diagnosed as *No anemia*, whereas they should not, based on their laboratory test results. Upon further inspection, we noted that all the misdiagnosed instances had values near the threshold value. In the *No anemia* misclassifications,

all the hemoglobin levels were close to the 13 and 12 g/dl thresholds for men and women, respectively (see Figure B.1). In particular, the hemoglobin of men had a mean of 12.982 (SD=0.011), while the one of women had a mean of 11.931 (SD=0.042). However, it should be noted that from a clinical point of view, hemoglobin levels close to the normal threshold usually do not lead to an anemia diagnosis. Similarly, looking at *Hemolytic anemia*, which had the lowest recall score at 0.94 (along with *Aplastic anemia*), 35 of its instances were diagnosed with *Vitamin B12/Folate deficiency anemia*. These instances had a mean MCV value of 99.765 (SD=0.170), thus close to the threshold of 100. The 11 other instances diagnosed with *Anemia of chronic disease* had a mean MCV level of 80.197 (SD=0.152), close to the threshold of 80. And the other 30 instances with an *Inconclusive diagnosis* all had values near the thresholds, but missing values for other features in the pathway leading to an inconclusive diagnosis.

Class Name	Precision	Recall	F1-Score
<i>Inconclusive diagnosis</i> (1344)	0.94	0.97	0.95
<i>Aplastic anemia</i> (1806)	1.00	0.94	0.97
<i>Hemolytic anemia</i> (1805)	1.00	0.94	0.97
<i>Iron deficiency anemia</i> (1679)	0.98	0.98	0.98
<i>Anemia of chronic disease</i> (1772)	0.99	0.97	0.98
<i>Unspecified anemia</i> (1793)	1.00	0.98	0.99
<i>Vitamin B12/Folate defic. anemia</i> (1801)	0.96	0.98	0.97
<i>No anemia</i> (2000)	0.92	1.00	0.96

Table 3: Classification report showing the detailed performance of the Dueling DQN-PER model. Classes of anemia diagnosis are reported with their respective support.

5.4. DQN Model Robustness

The DQN models also showed robustness to both noise and missing data, exhibiting a consistent performance throughout different levels of added noise and missing data. We believe that this is because DQN relies on neural networks that have been shown to be robust to noise in some cases (Goodfellow et al., 2016). This is due to the fact that adding noise to the training input can act as a form of regularization by preventing overfitting and leading to better generalization of the neural network. Likewise, neural networks have also demonstrated their capability to handle missing data as they are able to learn

the underlying representation of the data even with missing values. In this study, we remarked that introducing noise and missing data led to a decrease in performance of the *Inconclusive diagnosis* and *Iron deficiency anemia* classes (results not shown). This is attributed to the fact that some of the noisy instances and/or instances with missing data are being diagnosed with *Inconclusive diagnosis* instead of their anemia class, which is to be expected. In the real world, in such cases, clinicians may need to use their own judgment. Additionally, many *Anemia of Chronic Disease* instances are being diagnosed with *Iron Deficiency Anemia* because they are on the same branch of the tree. Regarding the datasets that have both additional noise and missing data, SVM performs much lower than the rest, and while DT performs better, its performance is still significantly lower than the other models. This can be attributed to decision tree sensitivity to noise and missing data. In addition, they are prone to overfitting, such that a slight change in the training dataset may lead to a different tree altogether. Alternatively, Random Forest builds multiple decision trees during their training process and is therefore less likely to overfit than the DT, making it more impervious to noise and missing data.

Finally, using the same hyperparameters for the model, the DQN model was able to perform consistently as the training set size gradually decreased. The reason for this is the same hyperparameters were used for the experiments therefore a smaller dataset just meant that the same experiences were sampled more often. However, there is still a loss in the information gained from the data, and therefore the smaller the dataset, the more varied the results as shown by the confidence interval in Figure 1(d).

Limitations One significant limitation of this study is the absence of experiments on a real-world dataset to evaluate our method. While the results from the synthetic dataset are very encouraging, and while we endeavor to reproduce imperfections of EHR data in our study, it is paramount that we test on real-world data. Additionally, the synthetic dataset used is not longitudinal. This initial study with anemia aimed to show the viability of the proposed method. Real-world EHR datasets often have a temporal dimension which will provide more insights into the progression of the pathways. Furthermore, with the availability of such data, we will be able to com-

pare our approach with models capable of handling sequential data, such as Recurrent Neural Networks.

Another limitation is the sole consideration of anemia, whose diagnosis follows a decision tree. Other conditions are diagnosed based on guidelines that do not follow a decision tree. It would require novel experiments to know to what extent our approach may be generalized to other kinds of diagnoses such as Systemic Lupus Erythematosus (SLE), which has a more complex diagnosis process. For such a condition, the design of the state space as well as the reward function may be more intricate, and may also require more advanced techniques.

Moreover, training the RL agents took a significantly longer time and used considerably more computing resources than the SOTA classifiers as shown in Table E.1. Also, the DQN model has many hyperparameters that would need to be further optimized. However, it should be noted that after model training, generating a diagnosis pathway for a test instance is trivial since the policy has already been learned by the model (see Table E.1).

Finally, we did not evaluate Large Language Model-based methods, which have shown promising results on other tasks. We will take them into consideration in future work.

6. Conclusion

In this work, we used DRL to generate personalized pathways for the diagnosis of anemia. We compared the performance of various DRL methods to each other and to state-of-the-art classifiers. We also tested the performance of DRL on noisy data, missing data, and on train sets of varying sizes. We demonstrated that our approach with DQN is suitable as it has a comparable performance with the SOTA classifiers with the added advantage of constructing personalized pathways for each patient. These pathways have the potential to guide the diagnosis of a new patient and to be aggregated to summarize possible pathways for a patient population. In future work, we aim to test our approach on different types of diagnoses, especially conditions whose diagnosis is not based on a decision tree. Additionally, since laboratory tests are usually ordered as a panel, this can be incorporated as well. It will also be interesting to test our approach on diagnoses that are not solely based on laboratory test results, but on multimodal data, potentially acquired over a significant period of time.

Finally, it will be crucial to assess our methods on real-world data.

Acknowledgments

This work is supported by the Inria CORDI-S Ph.D. program.

References

Julia Adler-Milstein, Jonathan H. Chen, and Gurpreet Dhaliwal. Next-Generation Artificial Intelligence for Diagnosis: From Predicting Diagnostic Labels to “Wayfinding”. *JAMA*, 326(24):2467–2468, 12 2021. ISSN 0098-7484. doi: 10.1001/jama.2021.22396. URL <https://doi.org/10.1001/jama.2021.22396>.

Karl Baker, Elaine Dunwoodie, Richard G Jones, Alex Newsham, Owen Johnson, Christopher P Price, Jane Wolstenholme, Jose Leal, Patrick McGinley, Chris Twelves, et al. Process mining routinely collected electronic health records to define real-life clinical pathways during chemotherapy. *International journal of medical informatics*, 103:32–41, 2017.

Greg Brockman, Vicki Cheung, Ludwig Pettersson, Jonas Schneider, John Schulman, Jie Tang, and Wojciech Zaremba. Openai gym. *arXiv preprint arXiv:1606.01540*, 2016.

Edward Choi, Mohammad Taha Bahadori, Andy Schuetz, Walter F Stewart, and Jimeng Sun. Doctor AI: Predicting clinical events via recurrent neural networks. In *Machine learning for healthcare conference*, pages 301–318. PMLR, 2016.

Marilyn J Field, Kathleen N Lohr, et al. Clinical practice guidelines. *Directions for a new program*, page 1990, 1990.

Ian Goodfellow, Yoshua Bengio, and Aaron Courville. *Deep learning*. MIT press, 2016.

Ashley Hill, Antonin Raffin, Maximilian Ernestus, Adam Gleave, Anssi Kanervisto, Rene Traore, Prafulla Dhariwal, Christopher Hesse, Oleg Klimov, Alex Nichol, Matthias Plappert, Alec Radford, John Schulman, Szymon Sidor, and Yuhuai Wu. Stable baselines. <https://github.com/hill-a/stable-baselines>, 2018.

Zhengxing Huang, Xudong Lu, and Hui long Duan. Latent treatment pattern discovery for clinical processes. *Journal of medical systems*, 37(2):1–10, 2013.

Zhengxing Huang, Wei Dong, Lei Ji, Chenxi Gan, Xudong Lu, and Hui long Duan. Discovery of clinical pathway patterns from event logs using probabilistic topic models. *Journal of biomedical informatics*, 47:39–57, 2014.

Zhengxing Huang, Zhenxiao Ge, Wei Dong, Kun-lun He, and Hui long Duan. Probabilistic modeling personalized treatment pathways using electronic health records. *Journal of biomedical informatics*, 86:33–48, 2018.

Jaromír Janisch, Tomáš Pevný, and Vilim Lisý. Classification with costly features using deep reinforcement learning. In *Proceedings of the AAAI Conference on Artificial Intelligence*, volume 33, pages 3959–3966, 2019.

Peter B Jensen, Lars J Jensen, and Søren Brunak. Mining electronic health records: towards better research applications and clinical care. *Nature Reviews Genetics*, 13(6):395–405, 2012.

Hao-Cheng Kao, Kai-Fu Tang, and Edward Chang. Context-aware symptom checking for disease diagnosis using hierarchical reinforcement learning. In *Proceedings of the AAAI Conference on Artificial Intelligence*, volume 32, 2018.

Ramisetty Kavya, Jabez Christopher, Subhrakanta Panda, and Y Bakthasingh Lazarus. Machine learning and xai approaches for allergy diagnosis. *Biomedical Signal Processing and Control*, 69:102681, 2021.

Małgorzata Koperska. Hematocrit / hemoglobin ratio calculator. <https://www.omnicalculator.com/health/hct-hgb>, 2023. Accessed: 2022-11-22.

Hiroshi Koshimizu, Ryosuke Kojima, Kazuomi Kario, and Yasushi Okuno. Prediction of blood pressure variability using deep neural networks. *International Journal of Medical Informatics*, 136:104067, 2020.

Tianhao Li, Zhishun Wang, Wei Lu, Qian Zhang, and Dengfeng Li. Electronic health records based reinforcement learning for treatment optimizing. *Information Systems*, 104:101878, 2022.

Yang Li and Junier Oliva. Active feature acquisition with generative surrogate models. In *International Conference on Machine Learning*, pages 6450–6459. PMLR, 2021.

Xijie Lin, Yuan Li, Yonghui Xu, Wei Guo, Wei He, Honglu Zhang, Lizhen Cui, and Chunyan Miao. Personalized clinical pathway recommendation via attention based pre-training. In *2021 IEEE International Conference on Bioinformatics and Biomedicine (BIBM)*, pages 980–987. IEEE, 2021.

Zachary C Lipton, David C Kale, Charles Elkan, and Randall Wetzel. Learning to diagnose with LSTM recurrent neural networks. *arXiv preprint arXiv:1511.03677*, 2015.

M.L. Littman. Markov decision processes. In Neil J. Smelser and Paul B. Baltes, editors, *International Encyclopedia of the Social & Behavioral Sciences*, pages 9240–9242. Pergamon, Oxford, 2001.

Riccardo Miotto, Li Li, Brian A Kidd, and Joel T Dudley. Deep patient: an unsupervised representation to predict the future of patients from the electronic health records. *Scientific reports*, 6(1):1–10, 2016.

Volodymyr Mnih, Koray Kavukcuoglu, David Silver, Andrei A Rusu, Joel Veness, Marc G Bellemare, Alex Graves, Martin Riedmiller, Andreas K Fidjeland, Georg Ostrovski, et al. Human-level control through deep reinforcement learning. *Nature*, 518(7540):529–533, 2015.

Faramarz Naeim, P. Nagesh Rao, Sophie X. Song, and Wayne W. Grody. 61 - disorders of red blood cells—anemias. In Faramarz Naeim, P. Nagesh Rao, Sophie X. Song, and Wayne W. Grody, editors, *Atlas of Hematopathology*, pages 675–704. Academic Press, 2013. ISBN 978-0-12-385183-3. doi: <https://doi.org/10.1016/B978-0-12-385183-3.00061-9>. URL <https://www.sciencedirect.com/science/article/pii/B9780123851833000619>.

Denise Nedea. Transferrin saturation calculator. <https://www.mdapp.co/transferrin-saturation-calculator-444/>, 2020. Accessed: 2022-11-24.

George Obaido, Blessing Ogbuokiri, Theo G Swart, Nimibofa Ayawei, Sydney Mambwe Kasongo, Kehinde Aruleba, Ibomoije Domor Mienye, Idowu

Aruleba, Williams Chukwu, Fadekemi Osaye, et al. An interpretable machine learning approach for hepatitis b diagnosis. *Applied sciences*, 12(21): 11127, 2022.

Adam Perer, Fei Wang, and Jianying Hu. Mining and exploring care pathways from electronic medical records with visual analytics. *Journal of biomedical informatics*, 56:369–378, 2015.

Tom Schaul, John Quan, Ioannis Antonoglou, and David Silver. Prioritized experience replay. *arXiv preprint arXiv:1511.05952*, 2015.

Matthew W Short and Jason E Domagalski. Iron deficiency anemia: evaluation and management. *American family physician*, 87(2):98–104, 2013.

Earl Steinberg, Sheldon Greenfield, Dianne Miller Wolman, Michelle Mancher, Robin Graham, et al. *Clinical practice guidelines we can trust*. national academies press, 2011.

Richard S Sutton and Andrew G Barto. *Reinforcement learning: An introduction*. MIT press, 2018.

Kai-Fu Tang, Hao-Cheng Kao, Chun-Nan Chou, and Edward Y Chang. Inquire and diagnose: Neural symptom checking ensemble using deep reinforcement learning. In *NIPS Workshop on Deep Reinforcement Learning*, 2016.

Hado Van Hasselt, Arthur Guez, and David Silver. Deep reinforcement learning with double q-learning. In *Proceedings of the AAAI conference on artificial intelligence*, volume 30, 2016.

Ziyu Wang, Tom Schaul, Matteo Hessel, Hado Hasselt, Marc Lanctot, and Nando Freitas. Dueling network architectures for deep reinforcement learning. In *International conference on machine learning*, pages 1995–2003. PMLR, 2016.

Christopher JCH Watkins and Peter Dayan. Q-learning. *Machine learning*, 8(3):279–292, 1992.

Zhongyu Wei, Qianlong Liu, Baolin Peng, Huaixiao Tou, Ting Chen, Xuan-Jing Huang, Kam-Fai Wong, and Xiang Dai. Task-oriented dialogue system for automatic diagnosis. In *Proceedings of the 56th Annual Meeting of the Association for Computational Linguistics (Volume 2: Short Papers)*, pages 201–207, 2018.

Zheng Yu, Yikuan Li, Joseph Kim, Kaixuan Huang, Yuan Luo, and Mengdi Wang. Deep reinforcement learning for cost-effective medical diagnosis. *arXiv preprint arXiv:2302.10261*, 2023.

Robert Zaiden. Evaluation of anemia. *BMJ Best Practice*, 2022. <https://bestpractice.bmjjournals.com/topics/en-us/93/diagnosis-approach>, Accessed: 2022-09-08.

Yiye Zhang, Rema Padman, and Nirav Patel. Paving the cowpath: Learning and visualizing clinical pathways from electronic health record data. *Journal of biomedical informatics*, 58:186–197, 2015.

Yazeed Zoabi, Shira Deri-Rozov, and Noam Shomron. Machine learning-based prediction of covid-19 diagnosis based on symptoms. *npj digital medicine*, 4(1):3, 2021.

Appendix A. Q-learning and its extensions

Q-learning (Watkins and Dayan, 1992) is an RL algorithm that outputs the best action to take in a given state based on the expected future reward of taking that action in that particular state. The expected future reward is named the Q-value of that state-action pair, noted $Q(s, a)$. At each time step, the agent selects an action following a policy π , and the goal is to find the optimal policy π^* that maximizes the reward function. During model training, the Q-values are updated using the Bellman Equation as follows:

$$Q(s_t, a_t) \leftarrow Q(s_t, a_t) + \alpha[r_{t+1} + \gamma \max_a Q(s_{t+1}, a) - Q(s_t, a_t)] \quad (4)$$

where α is the learning rate and γ is the discount factor that determines the importance of future reward relative to immediate reward.

In our use case, since the problem has a large state space, we propose to use a **Deep Q-Network (DQN)** (Mnih et al., 2015) which uses a neural network to approximate the Q-value function. A DQN comprises two networks of similar architecture, *i.e.*, the policy network, which interacts with the environment and learns the optimal policy, and the target network, which is used to define the target Q-value. At each time step, the policy network takes a state, s_t , as its input and outputs the Q-values for taking

the different actions in that state. The weights of the target network are frozen and updated at a specified interval by copying the weights of the policy network. The DQN algorithm learns by minimizing the loss function shown in Equation 5, where θ and θ^- represent the weights of the policy and target networks, respectively. Additionally, at each time step, a record of the model’s interaction with the environment (known as an experience) is stored in a memory buffer in the form $(s_t, a_t, r_{t+1}, s_{t+1})$.

$$L(\theta) = \mathbb{E}[(r_{t+1} + \gamma \max_a Q(s_{t+1}, a, \theta^-) - Q(s_t, a_t, \theta))^2] \quad (5)$$

In order to improve DQN stability and performance, several extensions of the DQN algorithm have been developed which we use in this paper and we briefly describe below:

Double DQN (DDQN) (Van Hasselt et al., 2016): The action is selected using the policy network, while the target network estimates the value of that action unlike in the standard DQN where the same network is used for both tasks. The loss function is thus modified as follows:

$$L(\theta) = \mathbb{E}[(r_{t+1} + \gamma Q(s_{t+1}, \arg \max_a Q(s_{t+1}, a, \theta), \theta^-) - Q(s_t, a_t, \theta))^2] \quad (6)$$

Dueling DQN (Wang et al., 2016): The Q-value function is split into two parts: a value function $V(s)$ that provides the value for being in that state, and an advantage function $A(s, a)$ that gives the advantage of the action a in the state s , as compared to the other actions. The two functions are then combined to get the Q values as shown in Equation 7.

$$Q(s, a) = V(s) + (A(s, a) - \frac{1}{|\mathcal{A}|} \sum_a A(s, a)) \quad (7)$$

where $|\mathcal{A}|$ is the total number of possible actions in that state.

Prioritized Experience Replay (PER) (Schaul et al., 2015): Each experience in the buffer is assigned a priority such that experiences that have a higher priority are sampled more often during training.

Appendix B. Dataset

B.1. Feature Inclusion

The first step of our dataset construction was the definition of a set of features, associated or not, with

anemia diagnosis. The hemoglobin level is the primary feature that is considered to determine whether a patient has anemia, therefore we included it in the dataset. Additionally, the normal level of hemoglobin varies between men and women, therefore gender was included too. We also included features from the decision tree of the standard guidelines for the diagnosis of anemia by Zaiden (2022). These include mean corpuscular volume (MCV), ferritin, reticulocyte count, segmented neutrophils and Total Iron Binding Capacity (TIBC). Additionally, we included features that are not in the tree, but that can be used to diagnose different types of anemia according to our discussions with a domain expert, namely, hematocrit, transferrin saturation (TSAT), red blood cells (RBC), serum iron and folate. Interestingly for our study, three of these features (hematocrit, TSAT and RBC) can be derived from other features and are accordingly correlated with features from our initial selection (e.g., hemoglobin and hematocrit). Furthermore, we added features that are not relevant to the diagnosis of anemia in order to observe their potential impact on the behavior of our model. These are creatinine, cholesterol, copper, ethanol, and glucose. Ultimately, a total of 17 features were included.

B.2. Dataset construction

The second step of the dataset construction was to build a dataset for 7 diagnosis classes. These are *No anemia*, *Vitamin B12/Folate deficiency anemia*, *Unspecified anemia*, *Anemia of chronic disease (ACD)*, *Iron deficiency anemia (IDA)*, *Hemolytic anemia*, and *Aplastic anemia*. Each anemia class dataset was built based on the decision tree represented in Figure B.1, which was manually constructed based on Zaiden (2022) and Short and Domagalski (2013).

For each class, the values of the features were generated using a uniform probability distribution whose parameters (minimum and maximum values) were determined through manual reviewing of the medical literature and thresholds of the decision tree in Figure B.1. Features that are correlated with other features were derived using known equations, that is, hematocrit (Koperska, 2023), TSAT (Nedea, 2020) and RBC (Naeim et al., 2013). 10,000 instances were created for each of the diagnosis classes, which were then combined to create a single dataset of 70,000 instances. Next, an eighth diagnosis class, *Inconclusive diagnosis* was created for when the model is not sure about the diagnosis of an instance. The *Inconclusive*

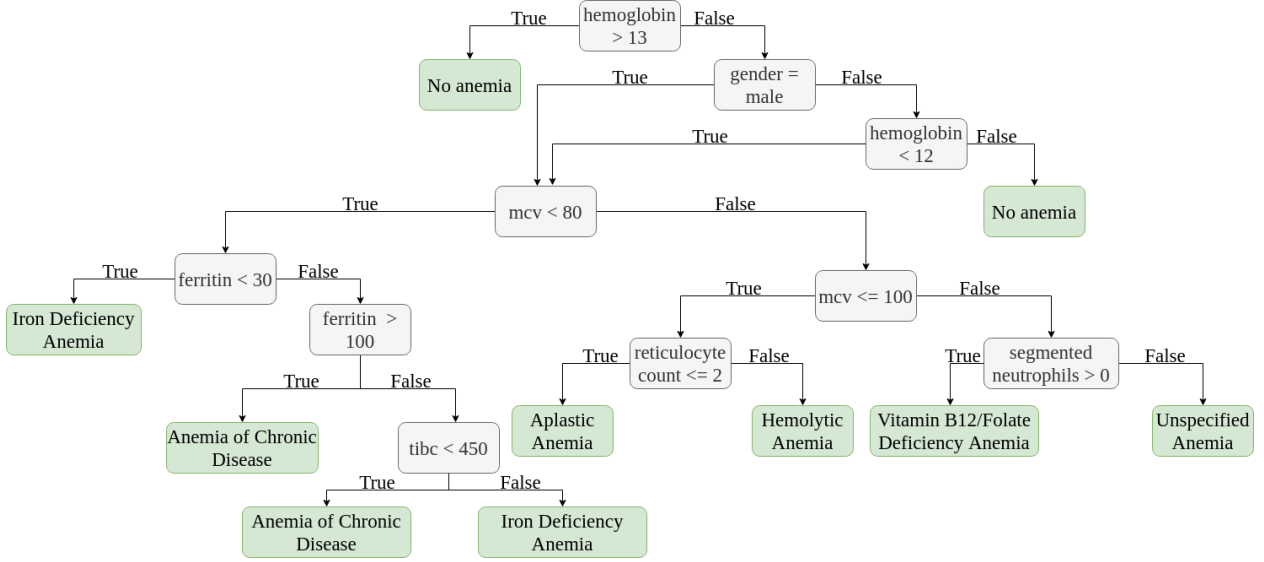


Figure B.1: The decision tree used to create the dataset as adapted from [Zaiden \(2022\)](#) and [Short and Domagalski \(2013\)](#).

diagnosis instances were created out of the existing 70,000 instances by randomly selecting and removing 10% of the non-missing values of each feature (except hemoglobin, gender and MCV, which are necessary to the diagnosis of almost all the anemia classes).

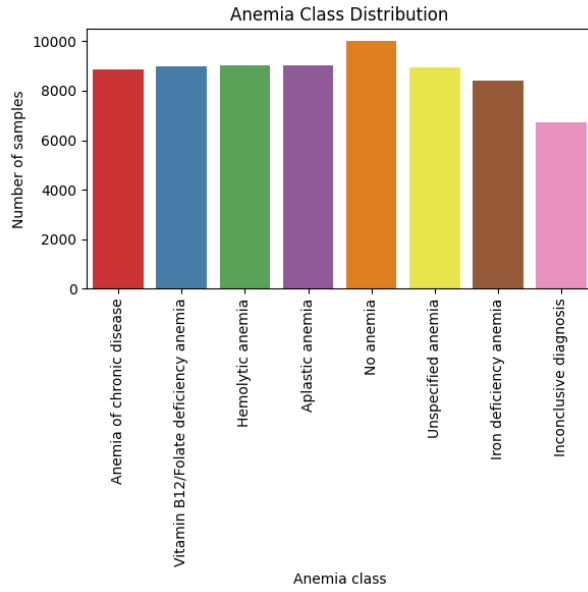


Figure B.2: Number of patients per anemia class.

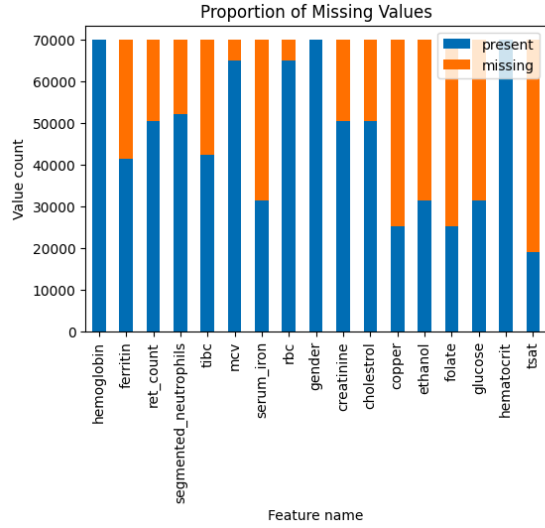


Figure B.3: Number of present vs missing values for each feature in the dataset.

B.3. Simulating Imperfect Data

To compare the robustness of various approaches to imperfect data, we artificially introduced different levels of noisiness and missingness to our training dataset.

Table B.1: Summary descriptive statistics of the dataset showing the mean and interquartile range (in parentheses) of the features. Gender, which is a binary variable, is described using the sample number and the percentage.

Feature	All Classes	No anemia	Vitamin B12/Folate deficiency anemia
Hemoglobin	10.239 (8.067, 12.102)	14.570 (13.281, 15.848)	9.510 (7.771, 11.274)
Ferritin	209.968 (69.870, 343.337)	251.436 (128.145, 373.501)	251.775 (126.676, 374.486)
Reticulocyte count	2.821 (1.270, 4.342)	2.981 (1.520, 4.423)	3.024 (1.526, 4.564)
Segmented neutrophils	2.930 (0.762, 4.898)	3.532 (1.824, 5.266)	3.516 (1.791, 5.22)
TIBC	334.276 (222.108, 457.942)	310.821 (206.744, 415.958)	306.678 (202.380, 410.634)
MCV	89.998 (78.918, 101.093)	90.029 (82.631, 97.598)	102.504 (101.225, 103.794)
Serum iron	135.030 (77.793, 192.645)	134.959 (76.979, 192.764)	136.613 (80.087, 193.071)
RBC	3.348 (2.641, 3.936)	4.899 (4.379, 5.356)	2.784 (2.274, 3.298)
Gender			
Male	38268 (54.67%)	4048 (40.48%)	5108 (56.73%)
Female	31732 (45.33%)	5952 (59.52%)	3896 (43.27%)
Creatinine	1.103 (0.651, 1.552)	1.119 (0.670, 1.566)	1.102 (0.655, 1.540)
Cholesterol	74.878 (37.388, 112.244)	74.037 (36.257, 111.019)	75.020 (37.099, 112.819)
Copper	80.095 (55.182, 105.245)	79.510 (54.965, 104.816)	80.001 (55.014, 105.150)
Ethanol	39.887 (19.876, 59.749)	40.256 (19.769, 60.865)	39.445 (18.622, 59.590)
Folate	15.262 (7.832, 22.715)	15.054 (7.843, 22.174)	15.400 (8.099, 22.976)
Glucose	90.039 (65.128, 115.077)	90.918 (66.287, 115.892)	90.021 (64.290, 116.194)
Hematocrit	30.716 (24.201, 36.306)	43.709 (39.843, 47.544)	28.530 (23.313, 33.821)
TSAT	49.601 (23.103, 62.608)	52.553 (24.626, 67.235)	53.935 (25.712, 68.534)

Feature	Unspecified anemia	Anemia of chronic disease	Iron deficiency anemia
Hemoglobin	9.534 (7.769, 11.301)	9.514 (7.751, 11.254)	9.539 (7.795, 11.276)
Ferritin	250.757 (123.567, 375.763)	268.551 (152.371, 384.475)	48.654 (22.742, 74.091)
Reticulocyte count	3.006 (1.546, 4.459)	2.957 (1.458, 4.457)	2.975 (1.441, 4.502)
Segmented neutrophils	0.000 (0.000, 0.000)	3.580 (1.848, 5.284)	3.582 (1.854, 5.330)
TIBC	311.332 (208.894, 414.291)	301.558 (199.155, 402.335)	452.223 (458.074, 499.101)
MCV	102.525 (101.274, 103.774)	77.472 (76.206, 194.049)	77.527 (76.299, 78.796)
Serum iron	134.970 (77.499, 192.216)	135.313 (77.093, 194.049)	135.625 (77.915, 193.272)
RBC	2.790 (2.274, 3.305)	3.685 (3.008, 4.361)	3.693 (3.013, 4.371)
Gender			
Male	5175 (57.73%)	5067 (57.20%)	4765 (56.74%)
Female	3789 (42.27%)	3792 (42.8%)	3633 (43.26%)
Creatinine	1.096 (0.643, 1.554)	1.098 (0.643, 1.544)	1.103 (0.643, 1.558)
Cholesterol	75.734 (38.838, 113.730)	74.994 (37.212, 112.230)	74.700 (37.507, 112.034)
Copper	80.465 (56.729, 105.069)	80.081 (54.461, 104.850)	79.764 (54.906, 104.545)
Ethanol	39.500 (19.102, 22.784)	39.784 (19.802, 59.703)	39.501 (20.018, 58.701)
Folate	15.284 (7.919, 22.784)	15.131 (7.769, 22.650)	15.462 (7.948, 22.976)
Glucose	89.457 (65.322, 113.808)	90.131 (66.091, 115.144)	90.153 (65.518, 114.407)
Hematocrit	28.602 (23.307, 33.902)	28.541 (23.253, 33.761)	28.617 (23.386, 33.828)
TSAT	52.689 (24.323, 67.385)	54.538 (24.730, 71.416)	32.675 (17.377, 42.591)

Feature	Hemolytic anemia	Aplastic anemia	Inconclusive diagnosis
Hemoglobin	9.510 (7.741, 11.262)	9.518 (7.801, 11.250)	9.486 (7.764, 11.224)
Ferritin	251.082 (123.988, 380.350)	246.611 (119.831, 374.303)	195.158 (67.362, 319.364)
Reticulocyte count	4.049 (3.079, 5.007)	1.005 (0.514, 1.500)	2.988 (1.437, 4.514)
Segmented neutrophils	3.553 (1.820, 5.271)	3.517 (1.789, 5.189)	3.478 (1.745, 5.214)
TIBC	310.197 (203.256, 418.237)	310.744 (205.529, 414.594)	338.282 (225.384, 461.215)
MCV	89.944 (84.920, 94.938)	89.985 (85.003, 95.013)	88.696 (78.100, 100.800)
Serum iron	133.068 (76.467, 191.047)	135.668 (79.215, 192.992)	133.704 (76.167, 191.807)
RBC	3.185 (2.580, 3.761)	3.186 (2.596, 3.747)	3.257 (2.628, 3.809)
Gender			
Male	5166 (57.24%)	5084 (56.31%)	3855 (57.36%)
Female	3859 (42.76%)	3945 (43.69%)	2866 (42.64%)
Creatinine	1.098 (0.656, 1.538)	1.100 (0.646, 1.551)	1.108 (0.646, 1.563)
Cholesterol	74.968 (37.216, 112.418)	74.990 (37.919, 112.314)	74.602 (37.416, 111.479)
Copper	80.348 (55.201, 105.698)	80.502 (55.372, 106.089)	80.166 (55.087, 105.649)
Ethanol	40.220 (20.430, 60.389)	40.525 (20.545, 60.523)	39.744 (21.113, 58.165)
Folate	15.396 (7.854, 22.746)	15.309 (7.731, 22.812)	15.045 (7.521, 22.613)
Glucose	90.140 (65.137, 115.555)	89.852 (64.575, 114.951)	89.348 (63.492, 113.911)
Hematocrit	28.530 (23.223, 33.785)	28.554 (23.402, 33.751)	28.458 (23.292, 33.671)
TSAT	53.800 (24.902, 69.688)	53.292 (26.181, 69.297)	48.753 (21.476, 63.018)

Table B.2: An instance in the dataset.

Feature	Value
Hemoglobin	9.007012
Ferritin	-
Reticulocyte count	-
Segmented neutrophils	3.519565
TIBC	440.499323
MCV	103.442762
Serum iron	59.017997
RBC	2.612173
Gender	Male
Creatinine	0.650757
Cholesterol	114.794964
Copper	112.308159
Ethanol	25.612786
Folate	5.969710
Glucose	116.026042
Hematocrit	27.021037
TSAT	13.397977
label	Vitamin B12/Folate deficiency anemia

For missingness, a percentage of the values for each feature, excluding hemoglobin and gender, were randomly replaced with missing values. Hemoglobin and gender were excepted because a patient’s hemoglobin level is key to the diagnosis of anemia and the normal levels of hemoglobin vary between men and women.

Since our original dataset perfectly follows a decision tree, we simulated noisiness using the following procedure. For each anemia class, except *No anemia* and *Inconclusive diagnosis*, a specified fraction of the values in each of the features in its branch of the tree in Figure B.1 were replaced by another value generated from a normal distribution, $N(\mu, \sigma^2)$, where the mean, μ , is the threshold in a node with that feature in the tree, and the standard deviation, σ , was defined by us.

For example, using hemolytic anemia, the features in its tree branch, that is, the features used to diagnose a patient with it are *hemoglobin*, *MCV* and *reticulocyte count* as shown in Figure B.1. Therefore, for a noise level of 0.2, we replaced 20% of the *reticulocyte count* values using a normal distribution function $N(2, 0.2)$ where $\mu = 2.0$ since this is the threshold in the decision tree. Similarly, for *MCV*, 10% of its feature values were replaced using a normal distribution $N(80, 2)$ while another 10% was replaced using a normal distribution function $N(100, 2)$. We gradually

increased the noise level fraction in order to analyze its effect on the performance of our model and the pathways it creates. Additionally, for all the noise levels, 10% of the anemic instances were randomly labeled as *No anemia*.

We further created datasets with both noisy and missing data. Using a training dataset with a noisiness level of 0.2 as described above, we added missing data at different levels to this dataset using the same procedure used to create the datasets with missing data.

Appendix C. Model Hyperparameters

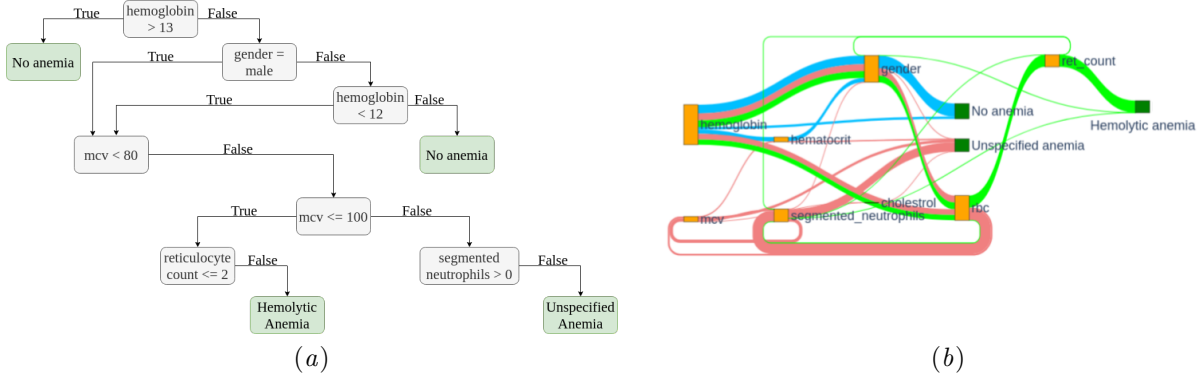
Table C.1 shows the values of the hyperparameters used for the DQN model in this study.

Appendix D. Sample Learned Pathways

Figures D.1 and D.2 provide examples of pathways generated with our approach. In particular, Figure D.1 is a side-by-side illustration of a branch of the decision tree used to label the dataset and a Sankey diagram showing the pathways learned by the Dueling DQN-PER model for the diagnosis of solely *No anemia*, *Unspecified anemia* and *Hemolytic anemia*,

Table C.1: DQN hyperparameter values.

Hyperparameter	Value
Buffer size	1000000
Learning rate	0.0001
Target network update frequency	10000
Learning starts	50000
Final epsilon value	0.05
Discount factor	0.99
Train frequency	4

Figure D.1: A side-by-side illustration of (a) a branch of the decision tree in Figure B.1 and (b) the corresponding pathways learned by the model for *No anemia*, *Hemolytic anemia* and *Unspecified anemia*.

which are colored *blue*, *coral* and *light green*, respectively. The value actions are represented by the orange nodes, while the diagnosis actions are the dark green nodes. In addition, the size of each flow corresponds to its support, *i.e.*, the number of patients that have it in their pathway. Figure D.2 shows the pathways learned by the model for the diagnosis of *Anemia of Chronic Disease* and *Aplastic anemia* which are colored *yellow* and *pink* in that order. One could enrich these visualizations with the threshold values that lead to one path or another.

Appendix E. Computing Time

In Table E.1, the time taken to train each model (training time), as well as, the time taken to generate a diagnosis pathway or a diagnosis (testing time) for the DQN models and the SOTA models respectively for a single instance in the test dataset are shown.

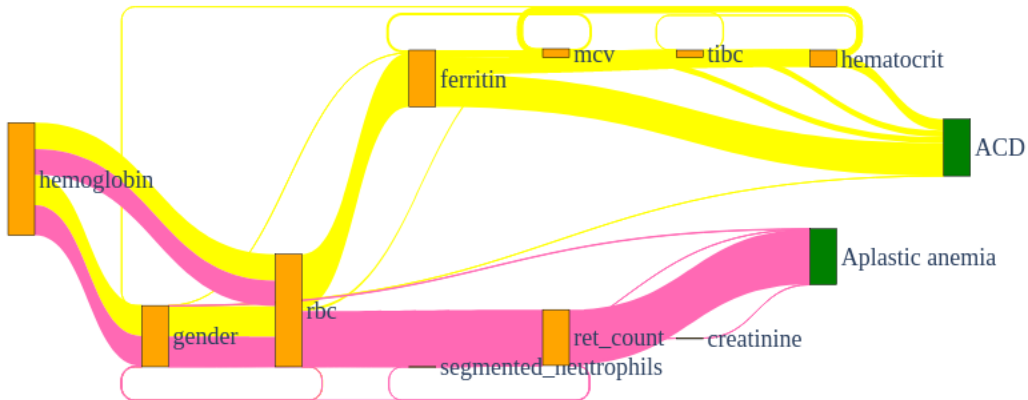


Figure D.2: The clinical diagnosis pathways for *ACD* and *Aplastic anemia* as learned by the agent.

Table E.1: The computing time to train the model and to generate a diagnosis (pathway) for a single test instance.

Model	Training time	Testing time
Decision Tree	299 ms \pm 9.72 ms	18.6 μ s \pm 453 ns
Random Forest	5.85 s \pm 8.56 ms	3.27 ms \pm 156 μ s
SVM	25.8 s \pm 437 ms	166 μ s \pm 8.33 μ s
FFNN	2min 36s \pm 35 s	645 μ s \pm 28.6 μ s
Dueling DQN-PER	1h 42 min 14s \pm 19 min 19s	722 μ s \pm 35.1 μ s
Dueling DDQN-PER	2h 12min 45s \pm 7min 36s	759 μ s \pm 56.1 μ s